Separation Science and Technology
Publication details, including instructions for authors and subscription information:
http://www.informaworld.com/smpp/title~content=t713708471

Ammonium Sulfate Crystallization in a Cooling Batch Crystallizer

Narayan S. Tavare[a]
[a] DEPARTMENT OF CHEMICAL ENGINEERING, UNIVERSITY OF MANCHESTER INSTITUTE OF SCIENCE AND TECHNOLOGY, MANCHESTER, ENGLAND

To cite this Article Tavare, Narayan S.(1992) 'Ammonium Sulfate Crystallization in a Cooling Batch Crystallizer', Separation Science and Technology, 27: 11, 1469 — 1487
To link to this Article: DOI: 10.1080/01496399208019437
URL: http://dx.doi.org/10.1080/01496399208019437

SEPARATION SCIENCE AND TECHNOLOGY, 27(11), pp. 1469–1487, 1992

Ammonium Sulfate Crystallization in a Cooling Batch Crystallizer

NARAYAN S. TAVARE

DEPARTMENT OF CHEMICAL ENGINEERING
UNIVERSITY OF MANCHESTER INSTITUTE OF SCIENCE AND TECHNOLOGY
P.O. BOX 88, SACKVILLE STREET, MANCHESTER M60 1QD, ENGLAND

Abstract

Crystallization kinetics of ammonium sulfate crystals are determined in a 25-L draft tube baffled, agitated crystallizer from a series of batch cooling experiments performed in an integral mode. The method of *s*-plane analysis for relative nucleation kinetics and the method of initial derivatives for growth rate kinetics are used to establish conventional kinetic expressions. A simulation technique is developed to calculate the product population density functions for the same system in a seeded cooling batch crystallizer configuration.

INTRODUCTION

In recent years considerable progress has been achieved in our understanding of batch crystallizers (*1*, *2*). Most of the previous work concerning batch crystallizer studies concentrates on isothermal operations either in extracting crystallization kinetics from experimental responses or in predicting crystal size distribution (CSD) from a known crystallizer configuration. The objective of the present work is to extract the crystallization kinetics from the experimental responses obtained from a seeded batch cooling crystallizer allowing temperature variation during the run. The second purpose of this communication is to present a simulation study of the same seeded batch cooling crystallizer. Systems having a large positive temperature coefficient of a solubility relation are normally crystallized in this way. Batch cooling crystallizers are widely used in the chemical industry. Ammonium sulfate, an important inorganic bulk chemical, was chosen for the present study.

The crystallization of ammonium sulfate has received considerable attention in recent years, and some progress has been made in determining

the applicable kinetic relationships. Mullin et al. (*3*) determined the nucleation kinetics using the Nyvlt method (*4*) as well as the growth rates of the two main faces of a single crystal in a flow cell. A nucleation order of 2.6 for dilute suspensions and first- and second-order growth kinetics for the (100) and (001) faces, respectively, of a crystal were reported. Both Chambliss (*5*) and Larson and Mullin (*6*) used MSMPR (mixed suspension mixed product removal) crystallizer experiments to deduce the relative kinetics of ammonium sulfate crystallization. A relative kinetic order of 1.5 and an exponent on magma density of unity were suggested. Larson and Mullin (*6*) found that traces of chromium ion suppress both nucleation and growth rates and modify the crystal habit. Youngquist and Randolph (*7*) investigated the secondary nucleation kinetics in a seeded continuous crystallizer by *in-situ* size analysis measurements with a Coulter Counter. A relative kinetic order of 1.22 and an exponent on magma density of 0.98 in a relative nucleation rate model were reported. Bourne and Faubel (*8*) suggested the use of mean product size variation to determine kinetic parameters and investigated the effect of impeller speed and material of construction on ammonium sulfate crystallization kinetics in two well-mixed, contoured base tanks of 1.7 and 42 L capacities. The relative kinetic order reported ranged from 1.6 to 2.5.

CRYSTALLIZATION KINETICS

Theory

The method of *s*-plane analysis can conveniently be used to establish the relative nucleation kinetics by determining both the crystal growth and nucleation rates simultaneously from a pair of experimental transient population density curves obtained from a perfectly mixed batch crystallizer (*9*). In this method a plot of the rate of change of the Laplace transformed population density against the product of the Laplace transform variable and average Laplace transformed population density over an optimal range of Laplace transform variable with respect to size yields a straight line with a slope that equals the negative of the average growth rate and an intercept nucleation rate at the average time of two curves.

A technique of using the initial derivatives evaluated from the initial portions of both supersaturation and temperature profiles obtained from a series of integral batch experiments provides experimental ease and flexibility to deduce the kinetic parameters in crystal growth correlations (*10*). The first two initial derivatives of supersaturation and temperature profiles with time can be determined from the second-order polynomial fit of experimental observations over the initial period of a run. The growth rate

order is the ratio of slope to intercept, and the activation energy is the negative ratio of the gas constant to the intercept, the linear regression being performed with variables determined from the initial derivatives. Although the technique is sensitive to experimental error in the measurement of initial supersaturation and temperature decay, the methods appear reasonably reliable and the accuracy of the resulting kinetic responses is probably comparable to that obtained using conventional techniques (*2*).

Experimental

In order to characterize the rate of processes in crystallization (viz., crystal growth and nucleation), a series of experiments was performed in a 25-L agitated draft tube baffled (DTB) vessel fitted with conical base baffle. Full details of the crystallizer, experimental procedure, and subsequent data reduction techniques have been reported in detail elsewhere (*10–12*). The experimental procedure used was similar to that used in isothermal experiments (*9*) except that the crystallizer was cooled from about 45 to 25°C during the run. In a typical run a hot, filtered solution of technical grade ammonium sulfate having a concentration corresponding to a saturation temperature of around 45°C was charged into the crystallizer. The solution was maintained initially at about 50°C by circulating hot water through the crystallizer draft tube. The solution was then cooled slowly to about 45°C. When the desired temperature is attained, presized, weighed, and cured seeds of uniform size (retained between two successive BSS sieves over the seed size range from 550 to 925 μm) were charged into the crystallizer, the overall crystal seed loading being about 20 kg/m^3 solution. Just before starting the run the heater in the circulating water thermostat bath was switched off and cooling water was fed to cooling coils in this batch started at a maximum rate. The circulating water in the bath was thus cooled at a slow rate, and this circulating water was used to cool the crystallizer contents. After running the crystallizer for 6000 s, the entire contents were removed and filtered, the product crystals air-dried, and a sieve analysis of product carried out.

The concentration of solution samples, taken at intervals throughout the batch, was determined by evaporating the samples to dryness, giving an estimated accuracy of better than $\pm 2 \times 10^{-4}$ kg salt/kg water. The supersaturation at any time was then estimated by subtracting the solubility from the actual solution concentration. The transient population density data were measured using a multichannel Coulter Counter (Model TAII with population count accessory) fitted with a 560-μm diameter Coulter orifice tube which enabled measurements to be made in the range of 17–200 μm. The final product size distribution was measured with BSS sieves so as to cover the size range 38–2000 μm.

TABLE 1
Ranges of Variables Covered During the Experimental Study

Initial temperature, °C	44–50
Final temperature, °C	27–31
Initial cooling rate, °C/s	−0.0033 to −0.0052
Initial concentration, kg salt/kg water	0.82–0.85
Final concentration, kg/salt/kg water	0.77–0.81
Supersaturation, kg salt/kg water	0.003–0.025
Initial supersaturation, kg salt/kg water	0.008–0.23
Stirrer speed, rev/s	8.3–14.7
Seed size, μm	550–925
Seed loading, kg salt/kg water	~0.03
Product magma density, kg salt/kg water	0.06–0.1
Weight mean product size, μm	1000–1300

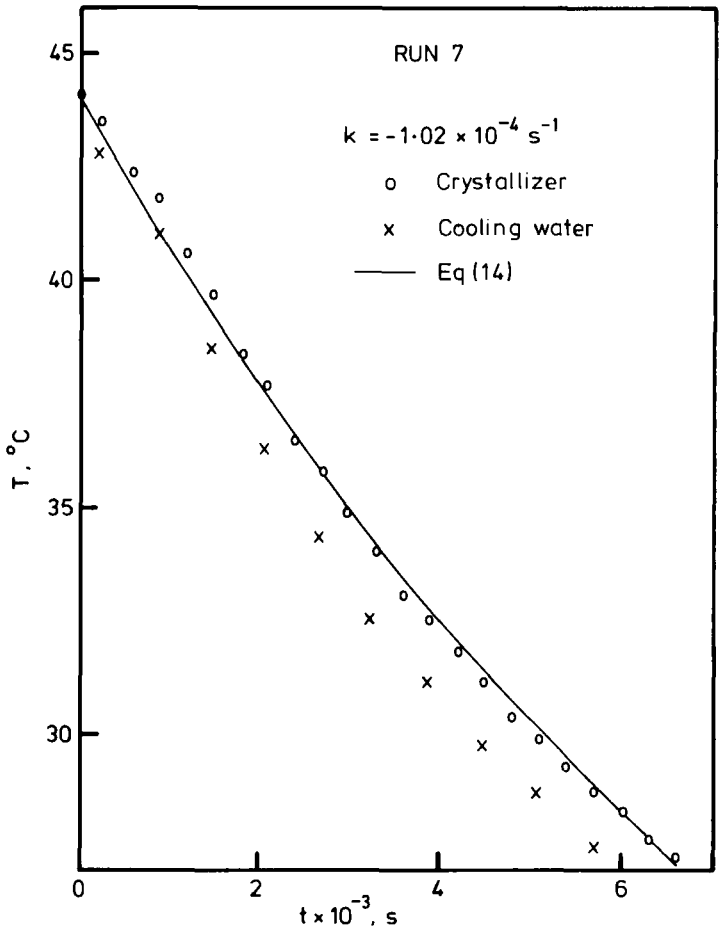

FIG. 1. Temperature variation.

Results and Discussion

A total of seven experiments was performed covering wide ranges of experimental conditions as reported in Table 1. Typical variations of temperatures, concentrations, and supersaturation for a run are shown in Figs. 1–3, respectively. Results obtained from the Coulter Counter measurements were used to calculate the growth and nucleation rates using the method of s-plane analysis. Typical results of population density curves for six samples are shown in Fig. 4. The method of s-plane analysis uses the differential approach. The parameters are assumed to be constant, representing the average over the sample time interval. In order to estimate average nucleation and growth rates over the optimal range of the Laplace transform variable, the linear regression in the method of s-plane analysis was performed using data from 50 points chosen at regular intervals of the Laplace transform variable over the range $(0,s_f)$, s_f being constrained by

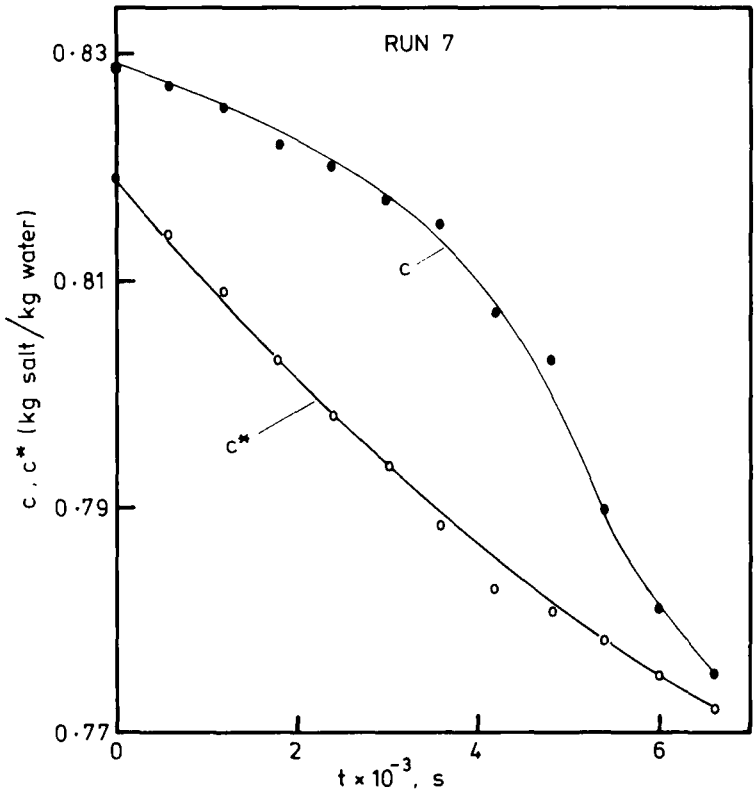

FIG. 2. Solution concentration profiles.

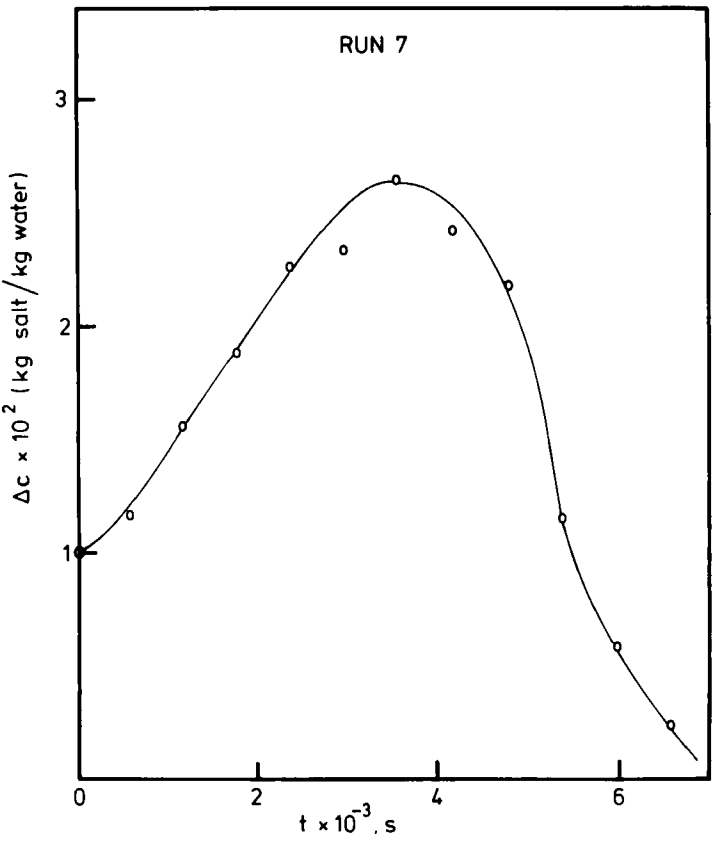

FIG. 3. Supersaturation variation.

$s_f\bar{L}_2 = 2$, where $\bar{L}_2$ is the population average size at time t_2. A typical linear plot for one pair of Coulter Counter experimental population density curves is given in Fig. 5 for $s_f\bar{L}_2 = 2$, only 10 data points equidistant on s being shown. All the results obtained from several runs using the method of s-plane analysis (with $s_f\bar{L}_2 = 2$) were correlated by an empirical power law for the relative nucleation kinetics as

$$B = K_R G^i M_T^j N^m \exp(-E/RT) \tag{1}$$

The growth rate kinetics correlation of the type

$$G = k_g \Delta c^g N^l \exp(-E_G/RT) \tag{2}$$

was determined from the same series of experiments using the method of initial derivatives (*10*). Note that T in the Arrhenius functional form is the

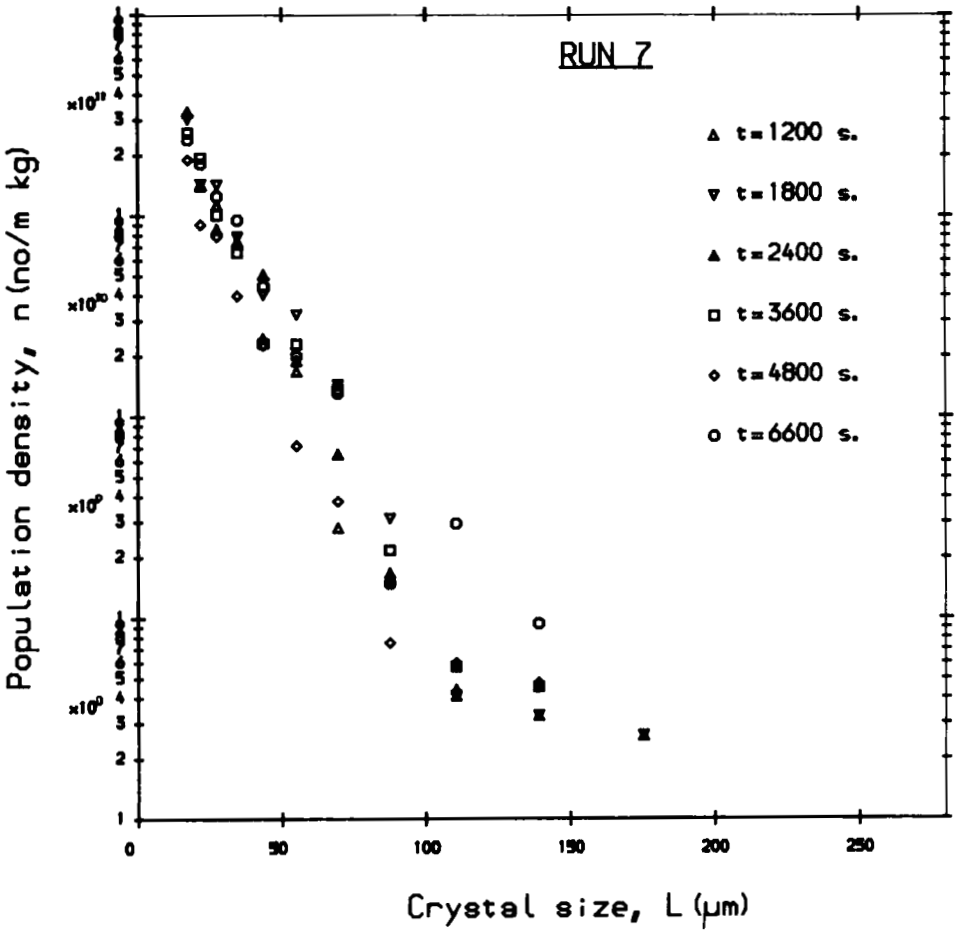

FIG. 4. Population density curves.

absolute temperature in K. The resulting parameter estimates are reported in Table 2, the typical process conditions used in Run 7 also being included. The form of Eqs. (1) and (2) is widely used to represent crystallization kinetics. The presence of G in the relative nucleation kinetics accounts for the effect of supersaturation on the nucleation process. Both growth and nucleation kinetic correlations show the effects of supersaturation, temperature, and stirrer speed. The magma density term in Eq. (1) accounts for secondary nucleation effects. Relatively high seed loading (~0.03 kg salt/kg water) was used throughout the experimental program to reduce the level of homogeneous nucleation.

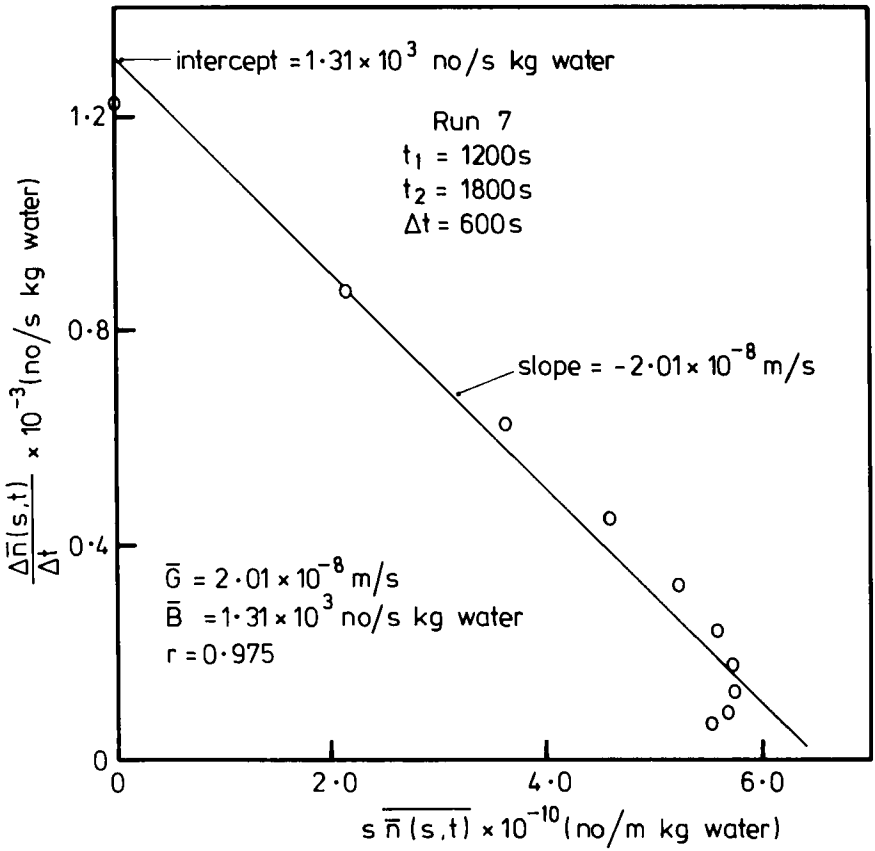

FIG. 5. s-plane analysis of experimental data (Fig. 4).

The important kinetic parameters (i and j) in Eq. (1) representing relative nucleation kinetics are estimated within reasonable confidence limits. The other less significant parameters, m and E, have a large variance, reflecting perhaps less significant variation of the corresponding variables during the experimental program. Both the significant parameters ($i = 0.84$ and $j = 0.42$) are somewhat lower than those reported in the literature by previous investigators [$i = 1.5$ and $j = 1$ by Chambliss (*5*), $i = 1.22$ and $j = 0.98$ by Youngquist and Randolph (*7*); $i \approx 1.5$–2.5 and $j = 1$ by Bourne and Fauble (*8*)]. The relative nucleation rate correlation as in Eq. (1) appears reasonable as the relative standard deviation in log and actual variables are 4 and 28%, respectively. Figure 6 shows the comparison of the relative nucleation kinetics correlations reported in the literature. Higher nucleation and lower growth rates are given from the work of Youngquist and

TABLE 2
Physiochemical Parameters and Process Conditions (Run 7)

ρ_c	=	1769 kg/m^3
ρ_s	=	1248 kg/m^3
ρ_{H_2O}	=	1000 kg/m^3
k_a	=	3.675
k_v	=	0.64
S_0	=	17.1 kg water
c_0	=	0.829 kg salt/kg water
T_0	=	44.1°C
T_w	=	10.0°C
k	=	-1.02×10^{-4} s^{-1}
W_0	=	0.5 kg
L_0	=	655 μm
τ	=	6600 s
N	=	13.25 rev/s
c^*	=	(0.00276T + 0.6972) kg salt/kg water where T is in °C
i	=	0.83 ± 0.05
j	=	0.58 ± 0.27
m	=	0.47
R	=	8.314 J/mol·K
E	=	15.23 ± 16.6 kJ/mol
K_R	=	3.0×10^{12} no/[kg·s(m/s)^i(kg/kg)^j(rev/s)^m]
g	=	0.91 ± 0.30
l	=	1.8 ± 2.6
E_G	=	61.85 ± 22.9 kJ/mol
k_κ	=	445.8 (m/[s(rev/s)^l(kg/kg)$^\kappa$]
L_{max}	=	500 μm
N_{grids}	=	500
M_{Ip}	=	0.075 kg salt/kg water
M_{Ts}	=	0.077 kg salt/kg water

Randolph (*7*) as they measured the CSD over the size range from 1.26 to 25.4 μm. Both Chambliss (*5*) and Larson and Mullin (*6*) determined their results from the sieve analysis over the size range 40 to 1500 μm. The present correlation, determined over the size range from 17 to 200 μm, appears in agreement with the trend in Fig. 6. All these different kinetics correlations seem to show some trend with the range of crystal sizes used in their derivation.

The growth rate order (g) in Eq. (2) has a reasonable standard deviation. The other parameters (l and E_G) appear to have large standard deviations. The parameters are extracted indirectly from a limited number of observations. Growth kinetics correlation (Eq. 2) shows a near first-order growth process similar to those reported by Mullin et al. (*3*) and Klekar and Larson (*13*); higher activation energy for the growth process (~60 kJ/mol) than

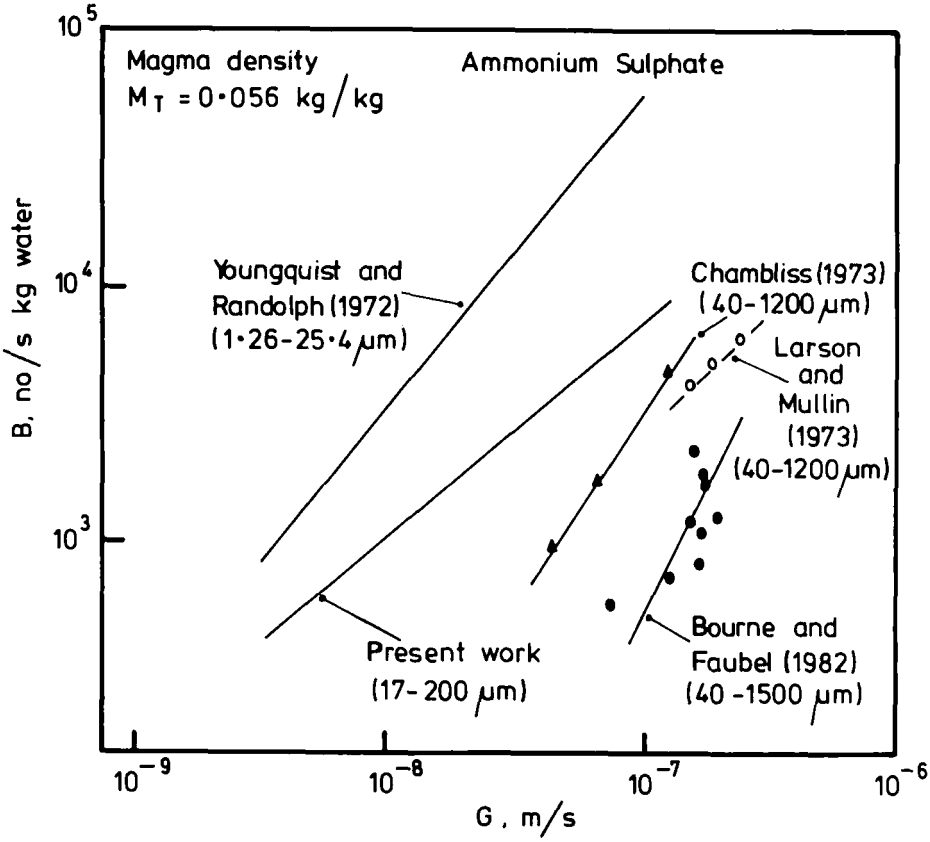

FIG. 6. Comparison of relative nucleation rate expressions.

that for the diffusional process (<~25 kJ/mol), and a strong, near second-order dependence on the stirrer speed. The overall growth rates predicted by Eq. (2) (~0.01–0.08 μm/s) compares favorably with the previous results (~0.02–0.25 μm/s) (*5*, *6*, *8*). Although the hydrodynamic environment influences the growth rate, as indicated by the strong dependence on stirrer speed, all the other observations and calculations tend to suggest that the growth rates appear to be controlled by the surface reaction step. The calculated rate constant in a simple power law correlation from Eq. (2) is at least one order of magnitude smaller than the mass transfer coefficient calculated from the empirical correlations (*14*, *15*). Previous studies for the present system (*3*, *6*) also reported surface reaction controlled growth. The assumption of size independent growth rate used for the present study

appears reasonable. On the basis of the correlations suggested by both Levins and Glastonbury (*14*) and Nienow (*15*), the diffusional transfer coefficient in an agitated vessel over most of a large particle size range is also a weak function of crystal size.

BATCH COOLING CRYSTALLIZER

Crystallization of ammonium sulfate was carried out in a seeded batch cooling crystallizer. For a perfectly mixed constant volume cooling crystallizer, the population balance equation for a system having size independent growth rate and negligible agglomeration and breakage is (*16*)

$$\frac{\partial n}{\partial t} + G\frac{\partial n}{\partial L} = 0 \tag{3}$$

The boundary condition for the nuclei population density can be represented as

$$n(t,0) = n^0 = B/G \tag{4}$$

The moment equations for the newly generated crystals, i.e., N crystals, obtained by moment transformation of the population balance (Eq. 3) with respect to size are

$$d\mu_0/dt = B \tag{5}$$

$$d\mu_1/dt = \mu_0 G \tag{6}$$

$$d\mu_2/dt = 2\mu_1 G \tag{7}$$

$$d\mu_3/dt = 3\mu_2 G \tag{8}$$

the initial moments for **N** crystals being zero.

In a batch crystallizer the specific rate of solid deposition per unit of mass of solvent for N crystals is

$$\frac{dW_N}{dt} = k_v \rho_c \frac{d\mu_3}{dt} = \frac{3k_v \rho_c}{k_a} A_N G \tag{9}$$

If the crystallizer is seeded at time $t = 0$ with crystals of narrow size distribution, for example, crystals retained between the two adjacent sieve

sizes differing by ΔL and having mean size L_0, the initial condition for the seeds, i.e., the S crystals, is

$$n(0,L) = f(L) = n_0 \Delta L \delta(L - L_0) \tag{10}$$

where n_0 is the initial population density having point value at L_0 determined by

$$n_0 = \frac{W_0}{\rho_c k_v L_0^3 \Delta L S} \tag{11}$$

The specific solid deposition rate for S crystals is

$$\frac{dW_S}{dt} = \frac{3W_0 L_S^2 G}{L_0^3 S} \tag{12}$$

The temperature–solubility relationship over the experimental range of temperature may be expressed empirically by the linear relation as

$$c^* = aT + b \tag{13}$$

The temperature variation of the crystallizer contents, i.e., the cooling curve starting from the initial temperature T_0, is represented by

$$dT/dt = k(T - T_w) \tag{14}$$

where k is the empirically determined characteristic constant of the crystallizer configuration. This cooling rate constant, k, represents a measure of heat transfer performance, i.e., the rate of heat transferred per unit of crystallizer heat capacity at a temperature difference of 1 K, and is characteristic of the process geometry and operating conditions.

The mass balance for this configuration can be written as

$$\frac{dc}{dt} + \frac{dW}{dt} = \frac{dc}{dt} + \frac{dW_N}{dt} + \frac{dW_S}{dt} = 0 \tag{15}$$

In a cooling crystallizer supersaturation is generated because of the reduction in solubility with temperature, and the supersaturation balance for this case will be

$$\frac{d\Delta c}{dt} + \frac{dc^*}{dt} + \frac{dW}{dt} = \frac{d\Delta c}{dt} + \frac{dc^*}{dT}\frac{dT}{dt} + \frac{dW}{dt} = 0 \tag{16}$$

Thus the supersaturation generation term can be defined from the solubility curve (Eq. 13) and the cooling curve (Eq. 14). The variation of seed crystal size in a batch crystallizer starting from $L = L_0$ at $t = 0$ as the initial condition may be represented as

$$dL_S/dt = G \tag{17}$$

Equations (3)–(17) mathematically represent the cooling crystallizer used in the present simulation study.

PROCESS SIMULATION ANALYSIS

In order to simulate the batch cooling crystallizer for ammonium sulfate crystallization from its aqueous solution, the set of equations (Eqs. 3–17) set out in the Batch Cooling Crystallizer Section was solved simultaneously for the specific parameters listed in Table 2.

All the differential equations (Eqs. 5–8, 14–17) were integrated by the fourth-order Runge Kutta method with an integration step length of 0.5 s with appropriate initial conditions mentioned in the Batch Cooling Crystallizer Section. The partial differential equation (Eq. 3) was solved by the modified method of numerical integration along the characteristics with a specified grid length of 1 μm. The set of eight differential equations (Eqs. 5–8, 14–17) was initially integrated with a step length of $\Delta t = 0.5$ s until the increment in size was equal to the size grid length of 1 μm used in the solution of the partial differential equation (Eq. 3). The growth rate and hence nuclei population density n^0 were defined at the end of the grid, and solution of the partial differential equation (Eq. 3) moved forward by the time required to increase the size by a one size grid length (1 μm). The calculated concentration profile showed rapid decay, resulting in a low level of supersaturation early in the run. This yielded a smaller size of the largest newly generated crystal than that observed. The calculations were therefore performed by using the observed supersaturation profile. A linear interpolation between the observations was used to determine the level of supersaturation at any intermediate time.

Temperature, Concentration, and Supersaturation Profiles

Variations of temperature, concentration, and supersaturation as used in the process simulation analysis of the experimental run are depicted by solid curves in Figs. 1–3, respectively. A reasonable agreement appears between the computed and observed temperature in the crystallizer. The cooling rate constant, k, used in Eq. (14) was determined from the observed temperature variation in the crystallizer for Run 7. The cooling rate for

the present configuration decreases slowly from 3.5×10^{-3} °C/s at the start to about 1.7×10^{-3} °C/s at the end. The heat of crystallization for ammonium sulfate crystals is about 11 kcal/kg of ammonium sulfate crystallized. The estimated average rate of solid deposition for Run 7 is around 7.0×10^{-6} kg/kg·s, and the estimated temperature change over the batch time due to this thermal effect, i.e., the heat of crystallization, is less than 0.5°C as compared to a total temperature change of about 20°C during the cooling process. The thermal effects due to the heat of crystallization for most inorganic salts are generally negligible. Also included in Fig. 1 is the temperature of the cooling water bath. The difference between crystallized and water bath temperatures at any time was always less than 2°C.

The decay in the observed concentration profile is slow initially and increases with time. Also included in Fig. 2 are the data points of saturation concentration corresponding to observed crystallizer temperatures and the saturation curve corresponding to the calculated temperature using Eq. (14). The solubility at any temperature was determined from the linear relationship (Eq. 13) over the experimental range of temperatures. The difference between the observed concentration and the saturation concentration is the supersaturation level prevailing at any time in the crystallizer. The rate of supersaturation generation in a cooling crystallizer is determined by the product of two derivatives, viz., solubility coefficient and cooling rate. As the constant temperature coefficient is used, the supersaturation generation rate varies with the cooling rate. This generated supersaturation is depleted mainly by the solid deposition on the surface of seed and newly generated crystals. The solid deposition rate on newly generated crystals increases slowly with the development of crystal size distribution of N crystals and is significant at the end of the batch. The contribution of the solid deposition rate on seed is substantial initially, passes through a maximum, and becomes less significant at the end of a run. The overall solid deposition rate thus passes through a maximum. The level of supersaturation prevailing at any time in a batch cooling crystallizer is determined by these two consecutive rate processes. The supersaturation for this cooling crystallizer passes through a maximum (Fig. 3).

Crystal Size Distribution

Although there is apparent scatter in observed results of population density data, typically as shown in Fig. 4, some trend in the movement of population density curves with time can be observed in most runs. A typical plot of the final product population density resulting from sieve analysis of the product crystals together with the final Coulter Counter

sample are depicted in Figure 7. The experimental data in this figure and most other runs illustrate the good agreement between the data points obtained with the Coulter Counter and by sieve analysis over the overlapping size range. The population density plot delineates clearly the two distinct parts representing the distributions due to nuclei (N crystals) and seeds (S crystals) in the product size analysis. Also included in Fig. 7 are the calculated population density curve for N crystals using the kinetic correlations and experimental supersaturation profile. The location of point population density as calculated by Eq. (11) at original seed size together

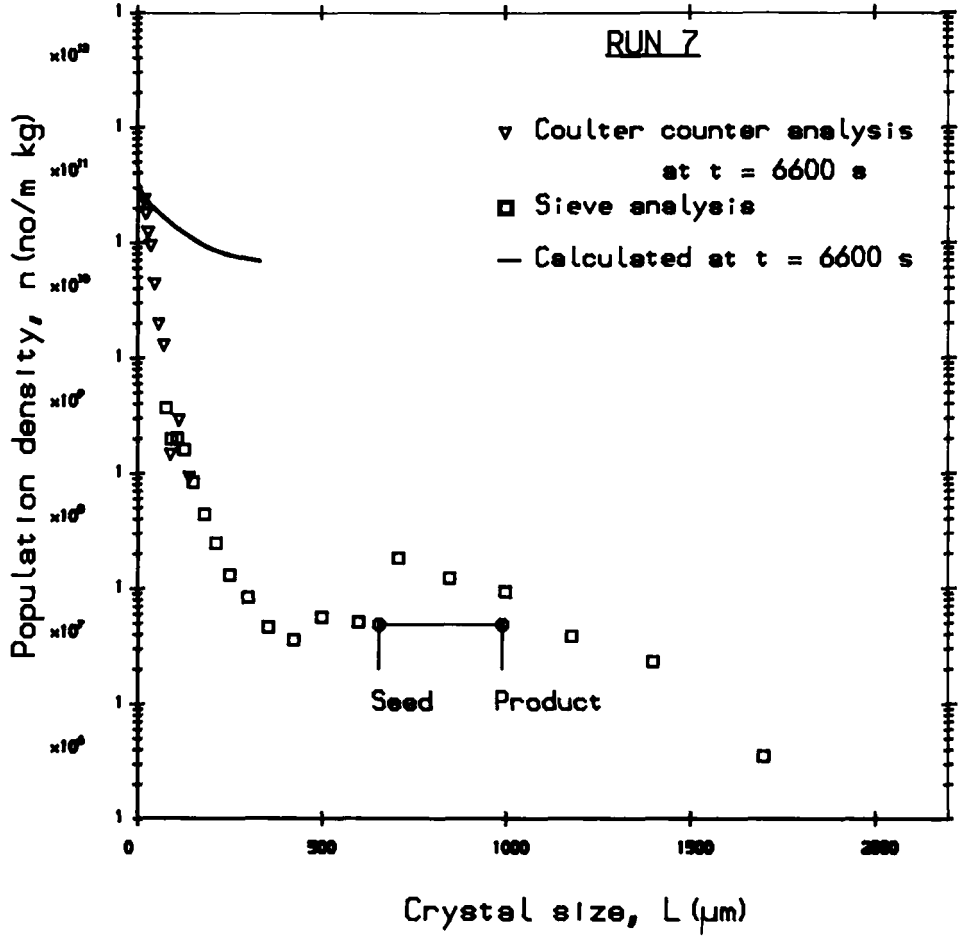

FIG. 7. Final product crystal size distribution:population density plot.

with the expected final size of the product for this run conditions is shown in Fig. 7. This shows a reasonable agreement with the two parts of measured product size distribution and confirms the reliability of growth kinetics. The wider spread in actual product size distribution as compared to narrow seed size distribution arises from the phenomenon of growth rate dispersion (*17*). The calculated maximum size of N crystals is about 330 μm and appears reasonable.

The calculated values of population density for N crystals are generally higher than those observed (Fig. 7), perhaps reflecting overprediction of nucleation rates (Fig. 6) as the growth rates were determined by the method of initial derivatives. The spread of the observed population density data is usually large as compared to calculated population density data. All these observations can be attributed to uncertainties associated with measurements of experimental responses, viz., population density and concentration measurements. During this run the ratio of maximum to minimum calculated growth rate from simulation is about 12.5 while that of nucleation rate is 5.2, and consequently the nuclei population density ratio is just ~4.8, which reflects in calculated population density curves. Measured population density curves show substantially higher changes than the calculated population density curves. Perhaps the kinetic correlations established from a limited amount of experimental data may not necessarily reflect the correct sensitivity of parameters describing the rate processes. Similar observations have been reported previously in batch potash alum crystallization and semibatch silica precipitation studies (*9*, *12*). However, in their simulation studies the kinetic parameters determined from the simulated noisy observations can be used to recalculate the original size distributions with a fair degree of confidence. The comparison of the calculated and observed population density curves perhaps illustrates a feature of calculation techniques based on moments. Because an averaging of the distribution is involved, it is difficult to invert the problem and recover the original data. Nevertheless, the process simulation analysis technique using simple process identification procedures to characterize the apparent rates of process occurring during the batch cooling crystallizer has been developed in this study. Such process simulation analysis studies will provide not only improved understanding of the process but also valuable information concerning the viability of the techniques used in extracting the kinetics from the experimental responses.

The consistency in the solute balances seems satisfactory as the suspension density calculated from the solutionside M_{Ts} using the initial and final concentrations in conjunction with the initial seed loading and that from the final product mass and hence solidside information, M_{Tp}, are in good agreement as seen in Table 2.

CONCLUSIONS

Crystallization kinetics of ammonium sulfate crystals were investigated in a 25-L DTB agitated crystallizer from batch cooling experiments performed in the integral mode using simple characterization techniques. The method of *s*-plane analysis was used to extract the kinetic rates from experimental transient population density data, and the results were correlated in terms of the conventional relative nucleation kinetics expression. Growth rate kinetics evaluated by the method of initial derivatives of supersaturation and temperature profiles with time for the same series of experiments were used. An algorithm to evaluate the transient crystal size distributions from a seeded batch cooling crystallizer was developed, and the results of crystal size distributions of product crystals were compared with the experimental observations. Process simulation analysis should be most useful in assessing the sensitivity of the kinetic and operating parameters to the performance characteristics of batch cooling crystallization systems.

NOMENCLATURE

a, b	constants in solubility relation (Eq. 13)
A	crystal surface area (m^2/kg water)
B	nucleation rate (no./kg water s)
c	concentration of solute (kg salt/kg water)
Δc	concentration driving force (kg salt/kg water)
E	relative nucleation activation energy (kJ/mol)
E_G	activation energy of growth process (kJ/mol)
$f(L)$	population density function of size (no./m·kg water)
g	growth order
G	overall linear growth rate (m/s)
i	relative kinetic order
j	exponent of slurry density
k	cooling rate constant (s^{-1})
k_a	surface shape factor
k_g	overall growth rate constant (m/[s(rev/s)^i(kg/kg)^g])
k_v	volume shape factor
K_R	relative nucleation rate constant (no.[kg·s(m/s)^i(kg/kg)^j(rev/s)^m])
l	exponent of stirrer speed in growth rate correlation (Eq. 2)
L	crystal size (m, μm)
ΔL	difference between successive sieve sizes (m, μm)
m	exponent of stirrer speed in nucleation rate correlation (Eq. 1)
M_T	suspension density (kg salt/kg water)
n	population density (no./m·kg water)

n^0 nuclei population density (no./m·kg water)
N stirrer speed rev/s)
N newly generated crystals
R universal gas constant (kJ/mol·K)
S solvent capacity of crystallizer (kg)
S seed crystals
t time (s)
T temperature (°C, K)
W weight of crystal (kg)

Greek Symbols

Δ difference
μ_k kth moment of crystal size distribution (no m^k/kg water)
ρ density (kg/m^3)

Subscripts

c crystal
f final
L at size L
N newly generated
0 initial value, seed
p product
s solution, solute
S seed

Superscripts

— average and the Laplace transformed quantity
* equilibrium
· derivative

REFERENCES

1. N. S. Tavare, J. Garside, and M. R. Chivate, "Analysis of Batch Crystallizers," *Ind. Eng. Chem., Process Des. Dev., 19*(4), 653–665 (1980).
2. N. S. Tavare, "Batch Crystallizers: A Review," *Chem. Eng. Commun., 61,* 259–318 (1987).
3. J. W. Mullin, M. Charkraborty, and K. Mehta, "Nucleation and Growth of Ammonium Sulphate Crystals from Aqueous Solutions," *J. Appl. Chem., 20,* 377–398 (1970).
4. J. Nyvlt, "Kinetics of Nucleation in Solutions," *J. Cryst. Growth, 3/4,* 377–398 (1968).
5. C. W. Chambliss, "Nucleation and Growth Kinetics in a Cooling Crystallizer," Ph.D. Thesis, Iowa State University, Ames, Iowa, 1966, cited in M. A. Larson and J. W. Mullin, Reference 6.
6. M. A. Larson and J. W. Mullin, "Crystallization Kinetics of Ammonium Sulphate," *J. Cryst. Growth, 20,* 183–191 (1973).

7. G. R. Youngquist and A. D. Randolph, "Secondary Nucleation in a Class II System: Ammonium Sulphate–Water," *AIChE J.*, *18*(2), 421–429 (1972).
8. J. R. Bourne and A. Faubel, "Influence of Agitation on the Nucleation of Ammonium Sulphate," in *Industrial Crystallization 81* (S. J. Jancic and E. J. de Jong, eds.), North Holland, Amsterdam, 1982, pp. 79–86.
9. N. S. Tavare and J. Garside, "Simultaneous Estimation of Crystal Nucleation and Growth Kinetics from Batch Experiments," *Chem. Eng. Res. Des.*, *64*, 109–118 (1986).
10. N. S. Tavare, "Growth Kinetics of Ammonium Sulphate in a Batch Cooling Crystallizer Using Initial Derivatives," *AIChE J.*, *31*(10), 1733–1735 (1985).
11. N. S. Tavare and J. Garside, *Crystallization Kinetics of Ammonium Sulphate in a Seeded Cooling Batch Crystallizer,* Research Report submitted to SPS, Harwell, 1983.
12. N. S. Tavare and J. Garside, *Reactive Precipitation in a Semi-Batch Crystallizer,* Presented at ICREC-II, Pune (India), 1987.
13. S. A. Klekar and M. A. Larson, *In-Situ Measurement of Supersaturation in Crystallization from Solution,* AIChE 66th Annual Meeting, Philadelphia, November 1973.
14. D. M. Levins and J. R. Glastonbury, "Particle–Liquid Hydrodynamics and Mass Transfer in a Stirred Vessel. Part II—Mass Transfer, *Trans. Inst. Chem. Eng.*, *50*, 132–146 (1972).
15. A. W. Nienow, "Agitated Vessel Particle—Liquid Mass Transfer: A Comparison between Theories and Data," *Chem. Eng. J.*, *9*, 153–169 (1975).
16. A. D. Randolph and M. A. Larson, *Theory of Particulate Processes,* Academic Press, New York, 1971.
17. N. S. Tavare, "Growth Rate Dispersion," *Can. J. Chem. Eng.*, *63*, 436–442 (1985).

Received by editor September 13, 1991